Title

New shielding configurations for a simultaneous PET/MRI scanner at 7T

Authors

Peng, Bo J
Wu, Yibao
Cherry, Simon R
et al.

Publication Date

2014-02-01

DOI

10.1016/j.jmr.2013.10.027

Peer reviewed

Published in final edited form as:
J Magn Reson. 2014 February ; 239: 50–56. doi:10.1016/j.jmr.2013.10.027.

New shielding configurations for a simultaneous PET/MRI scanner at 7T

Bo J. Peng[a,1], **Yibao Wu**[a], **Simon R. Cherry**[a], and **Jeffrey H. Walton**[b]

[a]Department of Biomedical Engineering, Unive rsity of California, Davis, Davis, CA 95616, United States

[b]NMR Facility, University of California, Davis, Davis, CA 95616, United States

Abstract

Understanding sources of electromagnetic interference are important in designing any electronic system. This is especially true when combining positron emission tomography (PET) and magnetic resonance imaging (MRI) in a multimodality system as coupling between the subsystems can degrade the performance of either modality. For this reason, eliminating radio frequency (RF) interference and gradient-induced eddy currents have been major challenges in building simultaneous hybrid PET/MRI systems. MRI requires negligible RF interference at the Larmor resonance frequency, while RF interference at almost any frequency may corrupt PET data. Moreover, any scheme that minimizes these interactions would, ideally, not compromise the performance of either subsystem. This paper lays out a plan to resolve these problems.

A carbon fiber composite material is found to be a good RF shield at the Larmor frequency (300 MHz in this work) while introducing negligible gradient eddy currents. This carbon fiber composite also provides excellent structural support for the PET detector components. Low frequency electromagnetic radiation (81 kHz here) from the switching power supplies of the gradient amplifiers was also found to interfere with the PET detector. Placing the PET detector module between two carbon fiber tubes and grounding the inner carbon fiber tube to the PET detector module ground reduced this interference. Further reductions were achieved by adding thin copper (Cu) foil on the outer carbon fiber case and electrically grounding the PET detector module so that all 3 components had a common ground, i.e. with the PET detector in an electrostatic cage. Finally, gradient switching typical in MRI sequences can result in count losses in the particular PET detector design studied. Moreover, the magnitude of this effect depends on the location of the detector within the magnet bore and which MRI gradient is being switched. These findings have a bearing on future designs of PET/MRI systems.

Keywords

PET/MRI; Multimodality; Shielding

Corresponding author: Jeffrey H. Walton: Phone: 1 (530) 752-7794; Fax: 1 (530) 752-0952 jhwalton@ucdavis.edu Address: 4303 Tupper Hall, University of California, Davis, CA, 95616..
[1]Present Address: PO Box 1450, Alexandria, VA 22313-1450

Introduction and background

The development of simultaneous positron emission tomography (PET) and magnetic resonance imaging (MRI) systems has received a great deal of attention [1, 2]. A combined PET/MRI system permits the acquisition of both functional and anatomic information while reducing the dose of ionizing radiation and offering better soft tissue contrast compared with a PET/computed tomography (CT) system. Many prototype PET/MRI systems have been developed. Some groups have used PET detectors based on traditional designs of scintillator crystals read out by photomultiplier tubes (PMTs) [3-8], typically with some form of fiber-optic coupling to reduce interference with the electron trajectories within the PMTs. Others systems have been developed with various designs of avalanche photodiodes (APDs) [9-11]. APDs are used in these systems instead of PMTs because the device characteristics and performance are largely unaltered by the presence of the magnetic field. APDs have lower gain than PMTs, thus the signals from APD-based systems and associated preamplifiers are especially sensitive to RF fields and thus require both good shielding and grounding.

Typically the shielding used to reduce RF interference is metallic, but metallic shielding introduces unwanted gradient-induced eddy current when the MRI is in operation [2]. The rapid switching of gradients can produce eddy currents in the shielding which adversely affects the quality of MR images if the geometry of the shielding produces a large conductive loop. Moreover, early prototype PET/MRI systems lacked the sensitivity and field of view compared to that of conventional PET systems. The next generation PET/MRI systems currently being developed will use additional detector rings and possibly incorporate depth of interaction information to improve system resolution and sensitivity. These additions of more detector material and electronics into the magnet bore will require a larger supporting structure and more metallic shielding. However, introducing additional metallic shielding into the system has the potential to increase gradient-induced eddy current effects, which could degrade MRI image quality [12, 13]. The purpose of the current paper is to find new ways to shield RF interference while reducing gradient-induced eddy current effects and at the same time maintaining the integrity of both systems' data acquisition. Two sources of RF interference need to be investigated when building a simultaneous PET/MRI system. One is RF interference generated at the Larmor frequency by the MRI RF coil (300 MHz on the 7T Bruker Biospec MR system used here). The other, less obvious source, is the RF generated by the switching power supply typically used in MRI gradient amplifiers (81 kHz here). In addition, the effects of gradient-induced eddy currents on the PET electronics are investigated. The implications for future construction of PET/MRI systems are discussed. Minimizing interactions in both directions are crucial to the development of high performance PET/MRI systems.

Several variations of metallic shielding are currently used to reduce RF interference in APD-based PET/MRI systems [9, 10, 14]. However, as previously reported, metallic structures close to the RF coil will degrade MR images. In order to minimize RF interference at 300 MHz while minimizing gradient-induced eddy currents, a careful study of RF shielding design is essential. Inserting breaks or slots in the metallic shielding or using a meshed shielding can help to reduce eddy currents while still providing sufficient electromagnetic shielding [12, 14]. However, epoxy impregnated carbon fiber composite materials have also been proposed as an effective RF shielding material [15-17]. Currently, most carbon fiber epoxy composites are constructed in a way that is both meshed and multi-layered [18]. They are MRI compatible and have very low magnetic susceptibility [19]. More importantly, they are characterized by relatively high DC electrical resistivity between 10^4 and 10^5 S/m^2, about 10^4 higher than the electrical resistivity of Cu [16, 20] Hence, much lower gradient-induced eddy currents are generated due to the inverse linear relationship between electrical resistivity and current. Carbon fiber composites are also strong, rigid materials, capable of

providing good structural support for the PET detectors and electronics. Therefore, these composites are very promising materials for constructing MR-compatible PET inserts.

Reducing RF interference at lower frequencies is also extremely important because such interference can lead to interference with the operation of the PET detectors. The MR gradient amplifiers on the 7T Bruker Biospec system used in this work are powered by a switching power supply, which generates and radiates 81 kHz RF. With no shielding, this RF significantly degrades the flood histogram (a 2D position map of photon interactions in the PET detector module) and the scintillator elements at the edges of the detector array cannot be resolved. However, carbon fiber tubing is only effective at shielding against high frequencies. Indeed, this property makes it useful as structural material that does not support eddy currents. Thus, the use of additional Cu foil and careful grounding to reduce this 81 kHz RF interference was also examined. In this paper, measurements of crosstalk between subsystems and analysis of flood and energy histograms from the PET detector show promising reductions in interference at 300 MHz and 81 kHz from the addition of the carbon fiber tubing and Cu foil respectively.

Eddy current effects were also studied to further validate the reduction of eddy currents with the new configuration when compared to an early prototype PET insert [9] and other shielding configurations [12]. Gradient switching interference was studied as well to identify potential interference in PET data acquisition. New evidence from gradient switching experiments suggests that PET data acquisitions should be synchronized with MRI pulse sequences in multimodality instruments in order to minimize data corruption. As a result of these findings, new shielding methodology is proposed.

Methods

A 7 T (300 MHz) Bruker Biospec MR system running ParaVision version 4 was used for this work. This system is equipped with three Copley 262NH amplifiers that drive the Magnex gradient set (model SGRAD MK III 180/120/S). The RF coil used in this work was Bruker's standard 35 mm ID mouse whole body resonator. The PET detector module consisted of an array of lutetium oxyorthosilicate (LSO) scintillator elements read out by a position-sensitive avalanche photodiode (PSAPD) [21]. Further details are in the supplementary materials.

Results and Discussion

RF shielding investigation at 300 MHz

The PET detector module was placed above the electrical center of a birdcage volume resonator -the standard 35 mm ID mouse volume coil supplied by Bruker - in order to mimic the final PET/MRI system design. The volume coil internal shield was sufficient that Q did not change when inserted into the various shields (see supplementary material). A single RF pulse at 300 MHz (duration 20 μs, repetition time 500 ms) was applied to the volume coil and relative coupling to the PET electronics measured. There was a relatively large coupling with no shielding (Figure 1, configuration 1). Various shields were placed around the volume coil and between it and the PET module. The power coupling from RF transmitter to the PET detector module electronics was reduced the most by the carbon fiber tube (configuration 5 of Figure 1). The experiment was repeated with much higher power and results were similar (see supplementary material). Adding additional Cu around the carbon fiber tube provided minimal improvement in shielding (configuration 5 vs. 6 in Figure 1). Using a much longer piece of carbon fiber tube, (596 mm vs. 151 mm) however resulted in a much better isolation (configuration 7 of Figure 1). We ascribe this additional shielding to

further coverage of the RF cable. The longer carbon fiber tube covered more of the RF cable, which was radiating 300 MHz.

Gradient shielding investigation at 81 kHz

The Copley gradient amplifiers used in this system have a switching power supply that operates at 81 kHz. The 81 kHz RF signal travels down the gradient cables into the magnet, and produces strong 81 kHz RF that significantly interferes with PET data acquisition. This interference varies with location and orientation of the PET detector module with respect to MRI gradient coil. Figure 2 shows the relative locations for the PET detector and shield for the 81 kHz shielding measurements and the gradient switching experiments below.

The measurements (see supplementary material for details) of the shielding efficiency at 81 kHz are in Figure 3. It is evident that the 81 kHz interference cannot be reduced with carbon fiber shielding alone or even with the addition of Cu shielding. However, placing the PET module between two carbon fiber tubes and electrically grounding the PET module to both the inner and outer carbon fiber tubes and covering the outer carbon fiber tube with Cu foil (configuration 4 of Figure 3) resulted in a dramatic reduction (47 db) in coupling. However this is still 18 dB above the baseline measure of -56 dB (Table S2, configuration 6) with gradient amplifier switched off.

It is important to note that an inner Cu shield is not necessary to reduce 81 kHz RF interference (Figure 3, configuration 4 vs 5). Eliminating the use of Cu shielding on the inner tube has the advantage of reducing gradient induced eddy currents, which can lead to MR signal degradation and image distortion. However, both carbon fiber tubes and proper grounding are crucial in reducing the 81 kHz RF interference.

Axial and azimuthal variations in the coupling were also investigated (see Supplementary Material and Figure S3 for details). Briefly, the maximum coupling is very close to isocenter demonstrating the need for excellent shielding. Furthermore there are variations in shielding efficiency with the orientation of the PET module inside the MRI bore. The gradient coil radiates 81 kHz when the amplifiers are powered on and the spatial variation results from the inherent structure of the gradient coil. These measurements enable us to choose the worst-case scenario for the rest of our studies. Moreover, this knowledge is necessary to design future PET/MR modules that will work at all locations inside the MRI bore with minimal interference.

The thickness of the outer Cu shield is also an important design criterion. 10 layers of copper were added for the measurements of Figure 3, however, beyond 7 layers, the shielding did not improve (data not shown). When this point is reached, the interference is not coming through the copper shielding in a radiative manner. Rather the voltage on the outer shield varies creating a potential difference between the shield and the PET module, which is grounded to the inner shield. The two structures form the plates of a capacitor with the potential difference varying at 81 kHz. This situation generates large interference on the detector. Building a ground plane between the gradient coil and PET module and providing a common ground reduces the potential difference between the detector and the two (inner and outer) carbon fiber tubes. Indeed, this is why configuration 4 of Figure 3 reduces the 81 kHz noise. This setup reduces the oscillating electric field at the position of the detector [22].

Energy spectra and flood histogram studies

The PET detector consists of an array of scintillation crystals. When the array is irradiated with an annihilation photon flood source (γ-rays), the electronic output signals from the photodetectors coupled to the crystal array can be used to compute the horizontal (X) and

vertical (Y) positions of the detected event. These X and Y positions are then histogrammed for a large number of detected events to provide a probabilistic map, where each peak corresponds to a single crystal in the detector array. This map is called the *flood histogram*. Spurious electrical signals on the detector circuitry can distort the coordinates of the detected event thus affecting the ability to identify the individual crystal peaks in the flood histogram and thus distort the PET image. Thus, energy (pulse-height) spectra and flood histograms were acquired from the PET detector module to determine whether shielding configurations reduce or eliminate degradation in determining the energy and location of detected PET events. The number of events detected by the PET detector module for a fixed radiation source per unit time also was compared under different conditions.

300 MHz—Energy spectra and flood histograms were acquired in the presence and absence of 300 MHz RF pulses. There were no significant differences in the flood histograms (Figure 4(a)) as seen from the profiles (4(b)) and the peak to valley Ratios (4(c)). or energy spectra (Figure 4(d)). This data further confirms that the carbon fiber tube shielding is capable of reducing RF interference at 300 MHz to levels similar to the noise level of the PET detector preamplifier. Furthermore, there was no change in counting rate on the detector when the 300 MHz RF was switched on (within the 0.7% precision allowed by the finite buffer size used to collect the data). Overall, carbon fiber is an excellent shielding material for 300 MHz.

81 kHz—Two sets of energy and flood histograms were again obtained from the PET detector module with the gradient amplifier power supply turned off and turned on. Flood histograms are shown in Figures 5(a) and (b). The reproducibility and variability of a given flood histogram is demonstrated in Figure 5(c) where the subtraction of two successive flood histograms, both with the gradient power supply off is shown. Figure 5(d) shows the subtraction of the flood histograms with the gradient power supply on and off, on the same scale. This difference image reveals a small shift of the locations on the crystal peaks when the power supply is switched on.

Response profiles of selected crystals, peak to valley ratios, and energy spectra with and without 81 kHz RF interference were measured (see supplementary material) and are similar to the RF results shown in Figure 4. There is a small broadening in the profile leading to a small but statistically significant decrease in the peak to valley ratio.

Figure 3 indicates that a small amount of 81 kHz interference still exists in the system after shielding (compare conditions 4 and 5 to 6). However, only a 0.09% difference was observed in the average number of events acquired by the PET detector when comparing sets of measurements taken with the gradient power supply on and off. Comparisons of flood histograms and energy spectra (Figures 4 and 5) demonstrate that this amount of residual interference will have a minimal affect on the performance of the PET detector module. Although flood histogram peak to valley ratios are generally lower when the gradient power supply is on, individual crystals are still readily identified in the flood histograms and there is expected to be little or no degradation in the resolution of the PET images. Furthermore, the energy spectra show no significant differences.

Gradient switching interference studies

Standard PET designs have rings of detectors to collect coincident γ rays thus placing them near the gradient coils in this design of a combined PET/MR system. During gradient ramp up and down, the changing magnetic field can produce electrical transients in the PET electronics potentially affecting PET data. Energy and flood histograms were obtained from

the PET module with the gradient system in 7 different states (see Table S3 and Supplementary Material for details).

Flood histograms and position profiles were again obtained for the same crystals as in Figure 4(a) with the best 81 kHz shielding configuration. The flood histograms are again similar except for small differences in their peak to valley ratios (see supplementary materials for details). Reductions in the peak to valley ratios (due to peak broadening) are mostly associated with the strength of the 81 kHz interference and vary little with gradient ramp time. The measured energy spectra were essentially identical and thus are not shown here. The number of counts recorded varies considerably depending on the proximity of the PET Detector to the gradient being switched. When the PET detector module is aligned with the center of the X gradient, the PET acquisition system loses more counts when the X gradient is switching than when the Y or Z gradient is switching and likewise more counts are lost when the detector is rotated to be aligned with Y and the Y gradient is pulsed (see supplementary material). Moreover, the strongest gradient strength and/or fastest gradient ramp-up time has the largest effect, likely because these conditions induce the largest eddy currents on the PET electronics. Switching the Z gradient has little impact on PET data acquisition in either case, possibly due to the geometry of the conducting paths, which are not conducive to supporting eddy currents induced by the Z gradient.

These data are consistent with the results of Catana et al. 2008 where a systematic decrease in counts with gradient switching was also observed. The maximum reduction in counts observed by the PET detector was ~2% with a gradient duty cycle of ~2%. This is a small effect here, however this admits the possibility that high gradient duty cycle MRI sequences such as RARE and EPI could have significant effects on PET counts.

In MRI sequences, the X and Y gradients seldom have any sort of time, amplitude, or duty cycle symmetry. Due to the orientational dependence of the counting losses observed, the effect on coincidence data will likely have some positional dependence and also will be strongly MR sequence dependent. This will complicate normalization of detector efficiencies across all the possible PET coincidence lines of response. To eliminate these effects it likely will be wise to gate the PET acquisition to the MRI sequence and avoid collecting PET data during times when rapid switching of high power gradients occurs. This will avoid PET data corruption resulting from the gradient-induced eddy currents on the PET electronic circuitry due to gradient ramp-up and ramp-down, at the expense of a small loss in effective sensitivity of the PET scanner. These effects will need extensive investigation and quantification that is beyond the scope of this work.

Eddy current evaluation with chemical shift imaging

A previously developed method based on chemical shift imaging (CSI) [12] was used to examine the effect of eddy currents with the current PET shielding configuration and compare with shielding results obtained previously. Briefly, in the CSI experiment, a large (80% of maximum) gradient pre-pulse with duration of 0.01 s was added to the beginning of a standard CSI sequence[12]. The time between this added gradient pre-pulse and the standard CSI pulse sequence was varied from 0.1 msec to 5 s. Eddy current effects were imaged by subtracting the reference field map (without the gradient pre-pulse) from data acquired with the gradient pre-pulse.

The PET detector module was again placed at the Z isocenter on the radius indicated in Figure 2. The best shielding configuration for 300 MHz and 81 kHz with the least copper (7 layers) was chosen. The results are shown in Figure 6. Peak shift images are shown in the left column with corresponding histograms in the right column. Results are shown for two different delay times. Figure 6 suggests that the impact of this shielding configuration, in

terms of Eddy current effects, is very small. It is much smaller than expected from traditional metallic shielding schemes. Furthermore, the magnitudes are similar to that previously observed with no shielding material[12]. This shielding configuration drastically reduces gradient-induced eddy currents, which is important as these can have a negative impact on MRI images.

Conclusions

There are significant interactions between the PET and MRI systems in a combined PET/MRI dual modality system and these interactions can affect the performance of both subsystems. Proper shielding requires particular care to minimize the interactions while not degrading performance.

This work has shown that the effects on the PET subsystem from the 300 MHz RF generated by the MRI can be effectively shielded by a carbon fiber epoxy composite tube. Power coupling measurements demonstrated that the 300 MHz was attenuated to almost the noise level in the PET subsystem. While this paper has not tested the carbon fiber at other frequencies, carbon fiber epoxy composites are effective because the carbon fibers are somewhat conductive with a conductivity of ~6 X 10^4 S/m^2. This translates to a skin depth of 0.12 mm at 300 MHz and 2.3 mm at 81 kHz. For clinical systems at 3T, the RF frequency is down by a little over a factor of 2 and thus carbon fiber epoxy is still expected to perform well, but this will require verification. In effect, the carbon fiber epoxy material is a low pass filter with the cutoff frequency set by the thickness of the carbon fiber material. Here, the choice of 3 mm of carbon fiber epoxy for these studies was more than sufficient if the criteria of 5 skin depths is used, but the number of skin depths required to adequately shield depends on the source amplitude. Thinner carbon fiber tubes are available from the manufacturer, but at some point structural and thermal stability become considerations as the PET detectors are significantly more efficient when cooled to ~5 °C [23]. Thus there is room for optimization but will require balancing these conflicting constraints.

Being able to also shield at 81 kHz is particularly important in this system due to interference from the switching power supply of the gradient amplifiers. Carbon fiber epoxy alone was not effective at shielding interference at 81 kHz coming from the power supplies of the gradient amplifiers. The presence of 81 kHz in the 7T MRI system caused a loss of counts in the PET detector module. However, to adequately shield at 81 kHz with carbon fiber epoxy composite alone would require an inordinately thick tube wall. The combination of a Cu shield on the outer carbon fiber tube while grounding the PET detector module to both the inner carbon fiber tube and the outer Cu shield significantly reduces this interference to a level at which the performance of the PET detector is not significantly degraded, though very small reductions in PET detector counting rate and flood histogram peak to valley ratios still exist. The grounding of the two carbon fiber tubes to the pet module ground form an electrostatic cage reminiscent of a Faraday cage. Without this grounding scheme, the PET detector module is sitting in an 81 kHz oscillating electric field.

Switching power supplies are relatively low cost and energy efficient and thus their use in the gradient amplifiers. In light of the results above, there are a couple of options for future designs of PET/MRI systems: 1) design gradient amplifiers with a different power supply – one without ripple on the output, 2) institute better filtering on the output such that ripple does not travel along the gradient cables to the magnet. Alternatively, the shielding design presented here appears to reduce the interference to acceptable levels using existing gradient amplifiers.

Measurements of PET counting events in the presence of gradient switching showed that there was a reduction in counts that was approximately the same as the gradient duty cycle. Furthermore, the loss of counts was dependent on the gradient applied and the azimuthal orientation of the detector about the MRI Z axis with respect to the gradient. The source of this reduction was unclear and will merit further study as high gradient duty cycle MRI sequences are frequently used. Gating of the PET acquisition may be necessary to avoid corruption of the PET data, albeit at the expense of loss in effective sensitivity of the PET scanner.

This new shielding configuration was also tested for effectiveness on the performance of the MRI subsystem. The CSI analysis showed that this configuration has a very low impact on MRI significantly reducing eddy currents when compared with previous designs[12]. This will permit the addition of more PET components while keeping their influence on the MRI subsystem to a minimum.

It should be noted that this work examined the interaction of a single PET detector module with a 7T (300 MHz) MRI system, which includes gradient amplifiers with switching power supplies operating at 81 kHz. In our experience in developing two previous PET/MR systems, the results from a single detector module are representative of what happens in a full PET insert, although there is the possibility that some effects may get worse (due to the increased number of components in the MR field of view), while others may get better (due to the symmetry of material in a ring of detectors versus a single detector module). It is expected that the RF performance of the shielding detailed here will work almost as well at the lower frequencies of clinical MRIs at 3T. However, shielding configurations and effectiveness will naturally depend on the specific MR system and on the specific pulse sequences used, nonetheless, the work presented here identifies sources of interference and provides strategies that should be broadly applicable for all laboratories developing hybrid PET/MR systems.

Supplementary Material

Refer to Web version on PubMed Central for supplementary material.

Acknowledgments

Support for this project was provided in part by NIH grants R01 EB000993 and RC2 CA148971. The MRI system was purchased from funds provided by NSF OSTI 97-24412.

References

1. Cherry SR, Louie AY, Jacobs RE. The integration of positron emission tomography with magnetic resonance imaging. P Ieee. 2008; 96:416–438.
2. Pichler BJ, Kolb A, Nagele T, Schlemmer HP. PET/MRI: Paving the Way for the Next Generation of Clinical Multimodality Imaging Applications. J Nucl Med. 2010; 51:333–336. [PubMed: 20150252]
3. Gilbert KM, Scholl TJ, Handler WB, Alford JK, Chronik BA. Evaluation of a Positron Emission Tomography (PET)-Compatible Field-Cycled MRI (FCMRI) Scanner. Magn Reson Med. 2009; 62:1017–1025. [PubMed: 19585601]
4. Mackewn JE, Strul D, Hallett WA, Halsted P, Page RA, Keevil SF, Williams SCR, Cherry SR, Marsden PK. Design and development of an MR-compatible PET scanner for imaging small animals, Nuclear Science. IEEE Transactions on. 2005; 52:1376–1380.
5. Poole M, Bowtell R, Green D, Pittard S, Lucas A, Hawkes R, Carpenter A. Split Gradient Coils for Simultaneous PET-MRI. Magn Reson Med. 2009; 62:1106–1111. [PubMed: 19780167]

6. Raylman RR, Majewski S, Lemieux SK, Velan SS, Kross B, Popov V, Smith MF, Weisenberger AG, Zorn C, Marano GD. Simultaneous MRI and PET imaging of a rat brain. Phys Med Biol. 2006; 51:6371. [PubMed: 17148823]
7. Shao Y, Cherry SR, Farahani K, Slates R, Silverman RW, Meadors K, Bowery A, Siegel S, Marsden PK, Garlick PB. Development of a PET detector system compatible with MRI/NMR systems. Ieee T Nucl Sci. 1997; 44:1167–1171.
8. Yamamoto S, Hatazawa J, Imaizumi M, Shimosegawa E, Aoki M, Sugiyama E, Kawakami M, Takamatsu S, Minato K, Matsumoto K, Senda M. A Multi-Slice Dual Layer MR-Compatible Animal PET System. Ieee T Nucl Sci. 2009; 56:2706–2713.
9. Catana C, Procissi D, Wu YB, Judenhofer MS, Qi JY, Pichler BJ, Jacobs RE, Cherry SR. Simultaneous in vivo positron emission tomography and magnetic resonance imaging. P Natl Acad Sci USA. 2008; 105:3705–3710.
10. Judenhofer MS, Wehrl HF, Newport DF, Catana C, Siegel SB, Becker M, Thielscher A, Kneilling M, Lichy MP, Eichner M, Klingel K, Reischl G, Widmaier S, Rocken M, Nutt RE, Machulla HJ, Uludag K, Cherry SR, Claussen CD, Pichler BJ. Simultaneous PET-MRI: a new approach for functional and morphological imaging. Nat Med. 2008; 14:459–465. [PubMed: 18376410]
11. Woody C, Schlyer D, Vaska P, Tomasi D, Solis-Najera S, Rooney W, Pratte JF, Junnarkar S, Stoll S, Master Z, Purschke M, Park SJ, Southekal S, Kriplani A, Krishnamoorthy S, Maramraju S, O'Connor P, Radeka V. Preliminary studies of a simultaneous PET/MRI scanner based on the RatCAP small animal tomograph. Nucl Instrum Meth A. 2007; 571:102–105.
12. Peng BJ, Walton JH, Cherry SR, Willig-Onwuachi J. Studies of the interactions of an MRI system with the shielding in a combined PET/MRI scanner. Phys Med Biol. 2010; 55:265–280. [PubMed: 20009193]
13. Yamamoto S, Watabe H, Kanai Y, Aoki M, Sugiyama E, Watabe T, Imaizumi M, Shimosegawa E, Hatazawa J. Interference between PET and MRI sub-systems in a silicon-photomultiplier-based PET/MRI system. Phys Med Biol. 2011; 56:4147–4159. [PubMed: 21693791]
14. Jihoon, K.; Yong, C.; Key Jo, H.; Jin Ho, J.; Wei, H.; Geun Ho, L.; Byung Jun, M.; Seung Han, S.; Yoon Suk, H.; Hyun Keong, L. Characterization of cross-compatibility of small animal insertable PET and MRI. In: Bo, Y., editor. IEEE Nuclear Science Symposium and Medical Imaging Conference (NSS/MIC 2009), Ieee; Orlando, FL. 2009; 2009. p. 3816-3821.
15. Chung DDL. Electrical applications of carbon materials. J Mater Sci. 2004; 39:2645–2661.
16. Keith JM, Janda NB, King JA. Shielding effectiveness density theory for carbon fiber/nylon 6,6 composites. Polym Composite. 2005; 26:671–678.
17. Kim T, Chung DDL. Mats and fabrics for electromagnetic interference shielding. J Mater Eng Perform. 2006; 15:295–298.
18. Jou WS. A novel structure of woven continuous-carbon fiber composites with high electromagnetic shielding. J Electron Mater. 2004; 33:162–170.
19. Reichenbach JR, Wurdinger S, Pfleiderer SOR, Kaiser WA. Comparison of artifacts produced from carbon fiber and titanium alloy needles at 1.5 T MR imaging. Jmri-J Magn Reson Im. 2000; 11:69–74.
20. Lind AC, Fry CG, Sotak CH. Measured electrical conductivities of carbon-fiber composite materials: Effects on nuclear magnetic resonance imaging. Journal of Applied Physics. 1990; 68:3518–3528.
21. Shah KS, Grazioso R, Farrell R, Glodo J, McClish M, Entine G, Dokhale P, Cherry SR. Position sensitive APDs for small animal PET imaging. Ieee T Nucl Sci. 2004; 51:91–95.
22. Cooper W, Daly C, Demarteau M, Fast J, Hanagaki K, Johnson M, Kuykendall W, Lubatti H, Matulik M, Nomerotski A, Quinn B, Wang J. Electrical properties of carbon fiber support systems. Nucl Instrum Meth A. 2005; 550:127–138.
23. Yang Y, Wu Y, Farrell R, Dokhale PA, Shah KS, Cherry SR. Signal and noise properties of position-sensitive avalanche photodiodes. Phys Med Biol. 2011; 56:6327. [PubMed: 21896961]

Highlights

- Subsystem coupling in a combined PET/MR small animal MRI is investigated.
- A grounding scheme is developed to increase isolation between the sub systems.
- Carbon fiber material provides good RF shielding without supporting eddy currents.
- Isolation also depends on the location of the PET electronics inside the gradients.
- Chemical shift imaging is used to image eddy current effects.

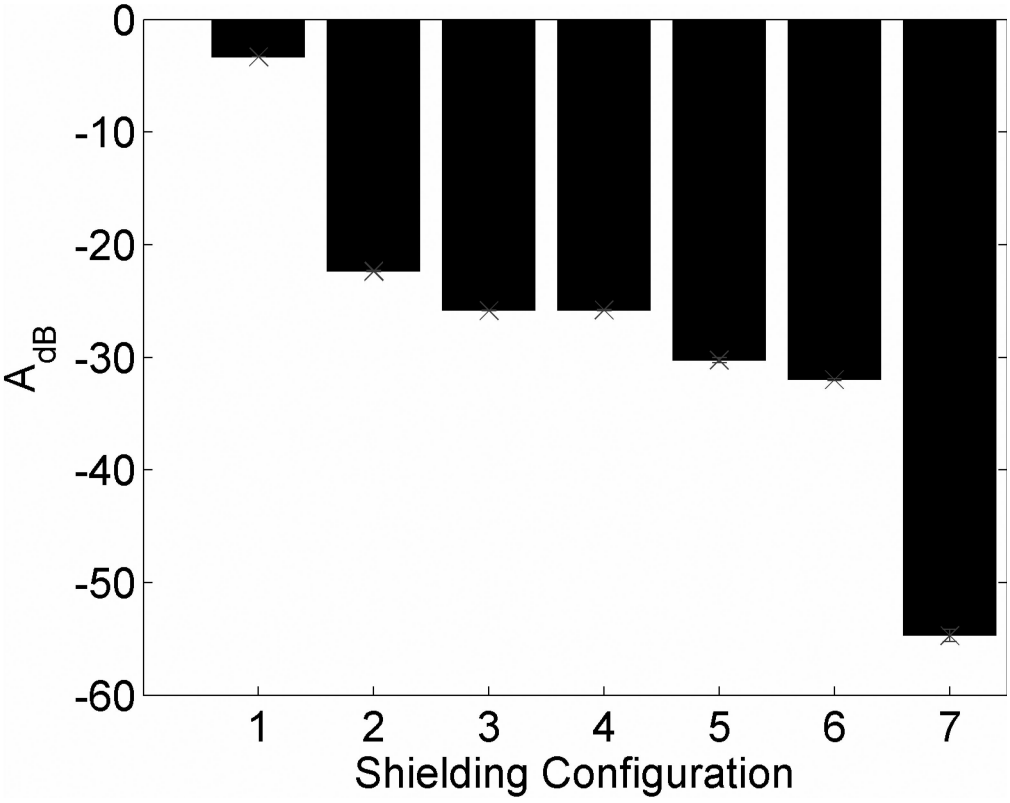

Figure 1.
Power coupling measurements for 300 MHz RF pulse. Attenuation of the RF pulse signal measured on the PET detector for 7 different shielding setups (Table S1 in Supplementary Material). Configuration 7, the carbon fiber tube provided the best shielding.

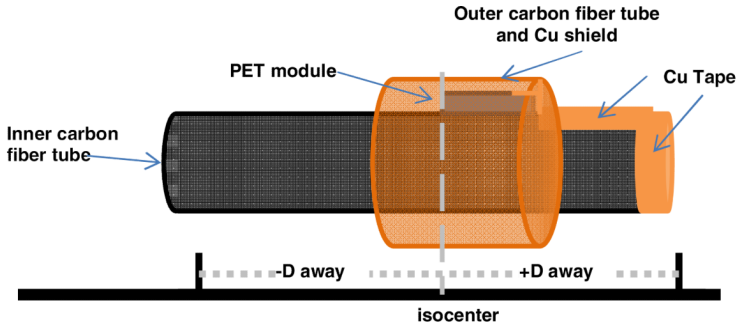

a

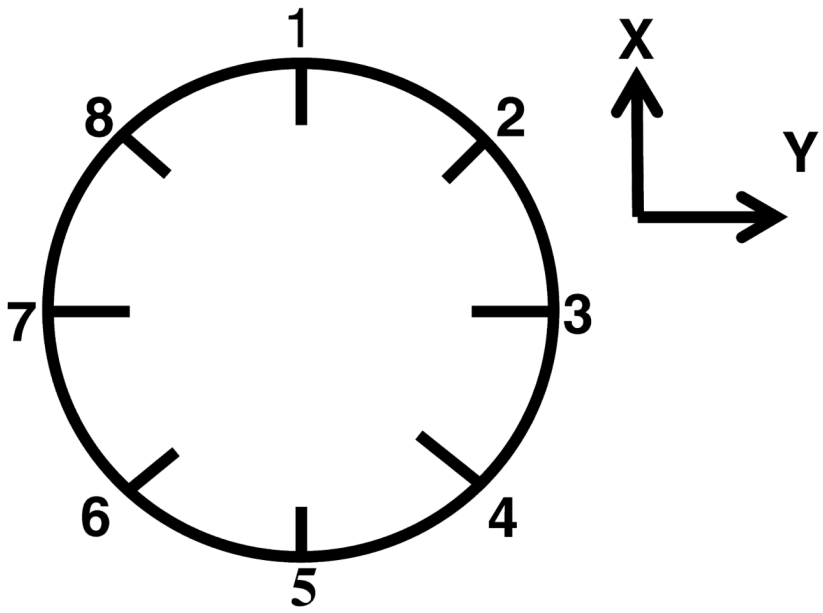

b

Figure 2.
Placement of PET detector module and its shielding structure with respect to (a) the MRI isocenter (axial location) and (b) the azimuthal location on the inner carbon fiber tube within the MRI system.

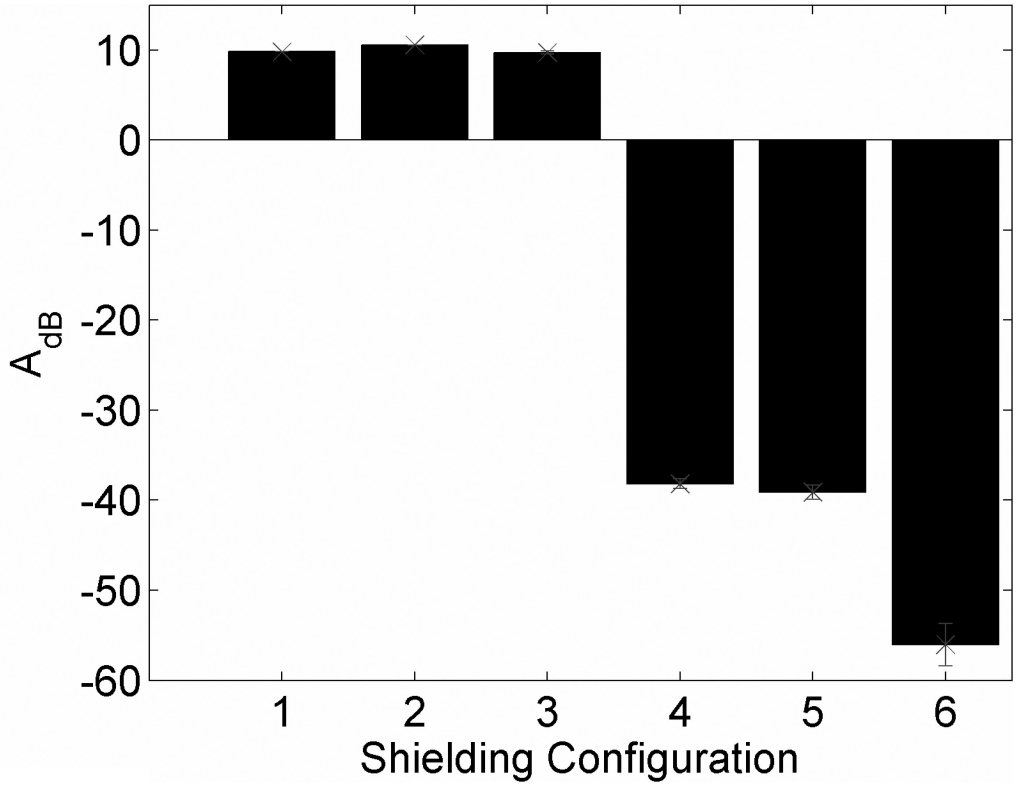

Figure 3.
Power coupling measurements for 81 kHz RF. Six different shielding configurations (see Table S2).

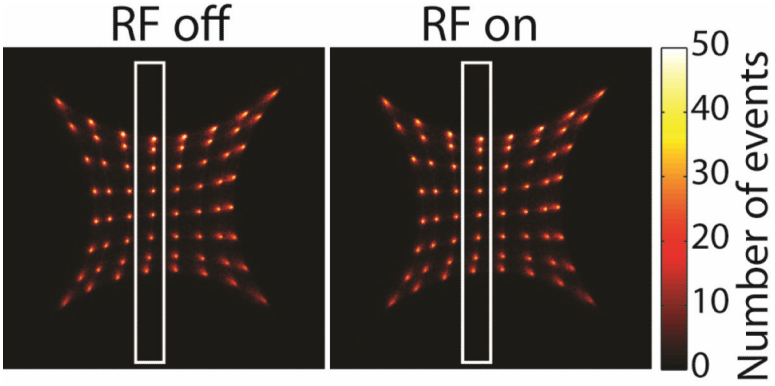

a

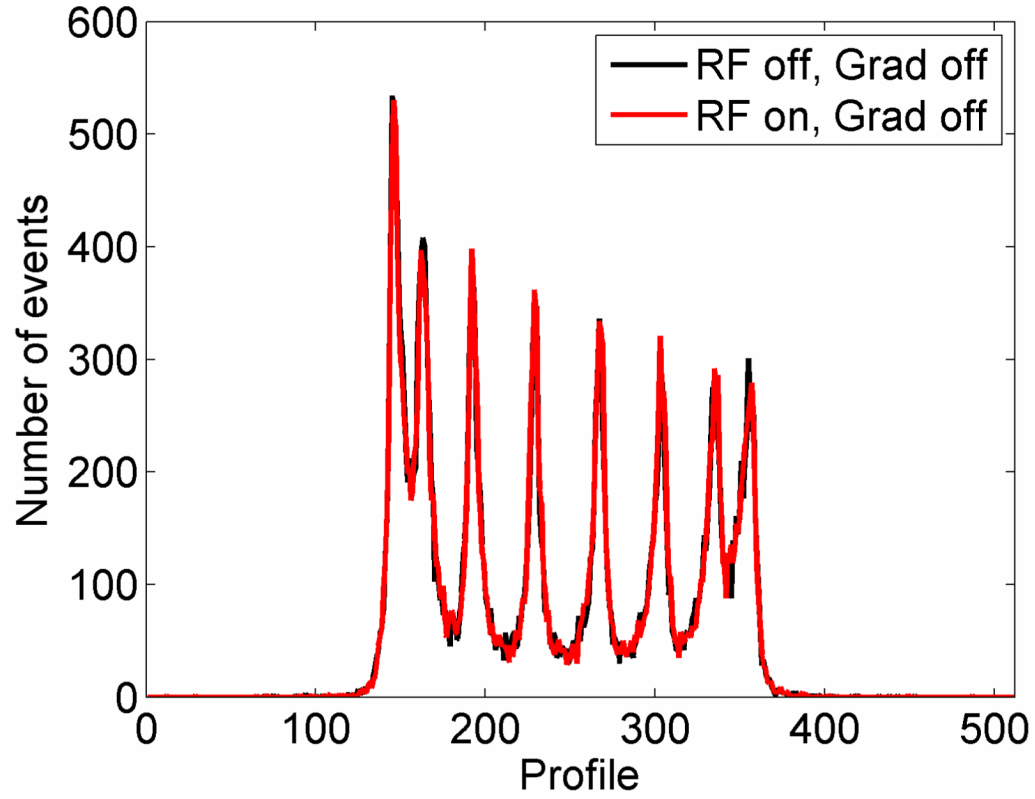

b

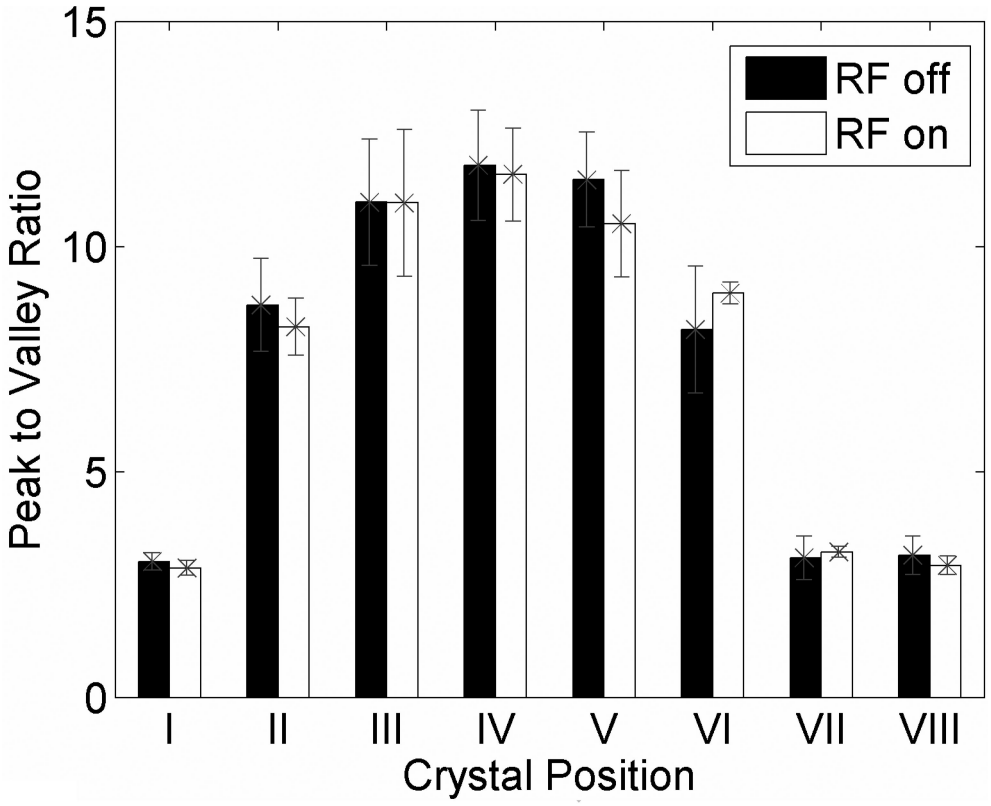

c

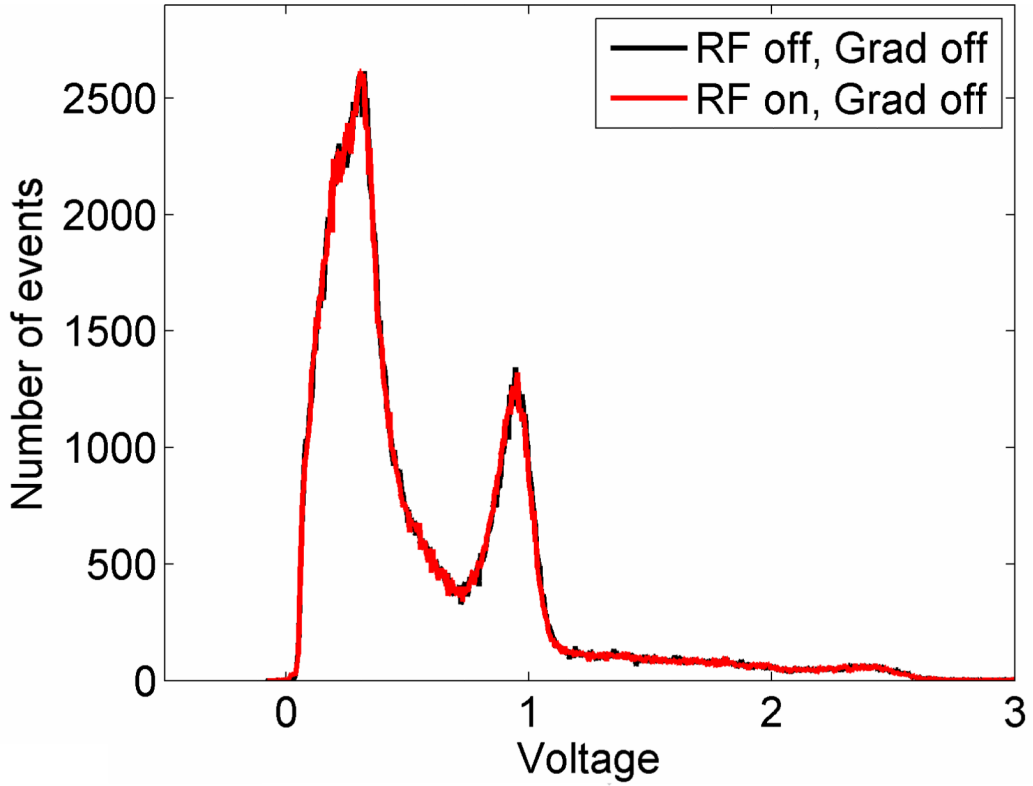

d

Figure 4.

(a) Flood histograms when the RF coil (300 MHz) was turned off (left) and on (right). (b) Profiles of the selected crystals (white box in (a)) from the flood histograms. (c) Peak to valley ratios of the profile. Error bars are standard deviations. (d) Energy spectra when the RF coil was turned off (black) and on (red).

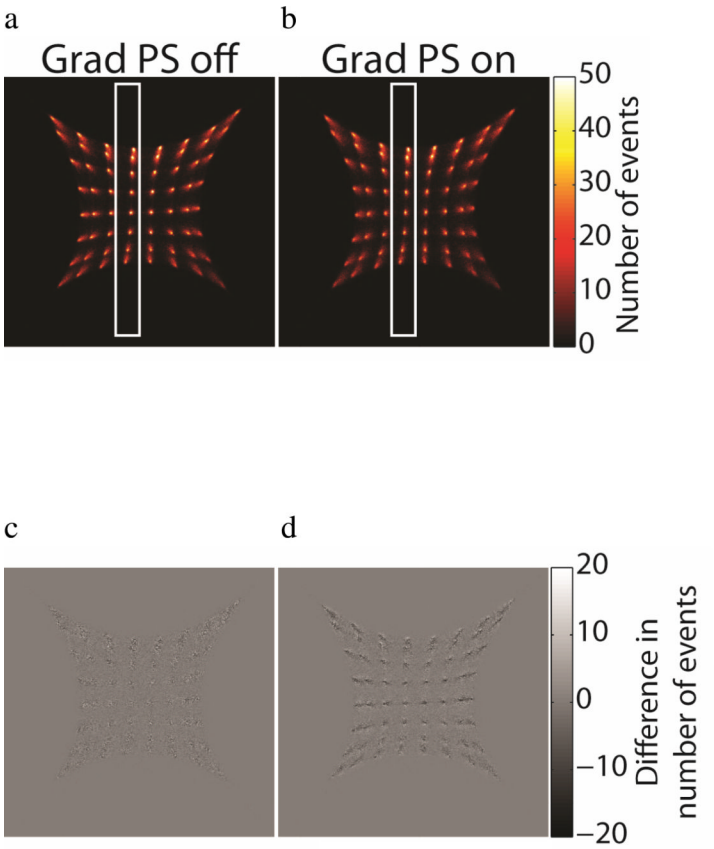

Figure 5.
Flood histograms when gradient power supply (81 kHz) was turned off (a) and on (b). (c) Subtraction of the two sequential flood histograms acquired when gradient power supply was turned off. (d) Subtraction of the flood histograms in (a) and (b). White boxes in (a) and (b) encompass the 8 detector crystals used for extracting the profiles (supplementary material).

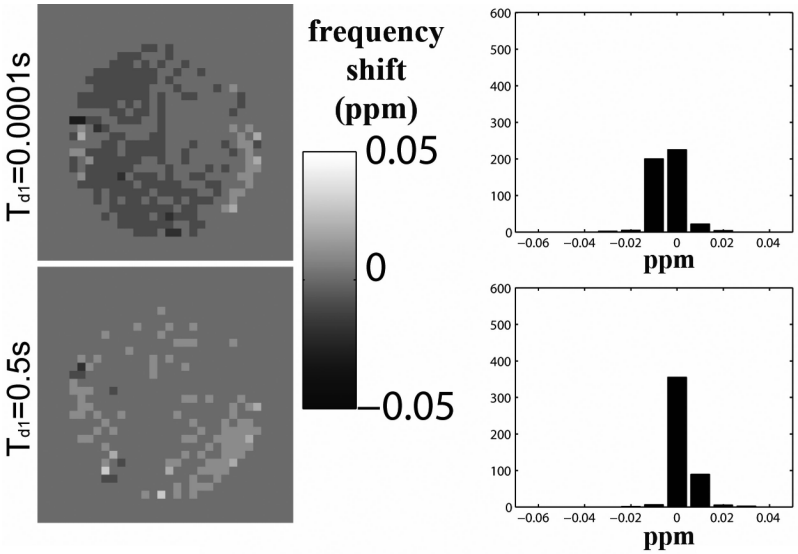

Figure 6.

CSI data gives a visual representation of induced eddy current fields with this new shielding configuration. (a) Maps of the pixel-by-pixel shift in resonance frequency for the CH_2 peak of ethylene glycol resulting from the gradient pre-pulse. The shift is from resonance frequency with no pre-pulse applied. Two different pre-pulse delay times are shown. (b) Histograms of the frequency shifts shown in (a).